

Correlation of dislocation and domain structure of Cr(001) investigated by spin-polarized scanning tunneling microscopy

R. Ravlić, M. Bode, A. Kubetzka, and R. Wiesendanger

Institute of Applied Physics and Microstructure Research Center, University of Hamburg, Jungiusstrasse 11, D-20355 Hamburg, Germany

(Received 20 November 2002; published 16 May 2003)

The Cr(001) surface has been investigated by spin-polarized scanning tunneling microscopy to image various defects and their effect on the magnetic structure at the surface. The usual magnetic structure is determined by the antiferromagnetic ordering of Cr leading to the topological antiferromagnetism of the (001) surface. We found that screw dislocations result in the formation of domain walls with a width of 120–170 nm. The dependence of the domain-wall width on the distance from the screw dislocation is studied experimentally and compared to micromagnetic simulations. Our results show that the size and shape of the spin structure is determined by two parameters, the exchange stiffness and the effective anisotropy. Subsurface step dislocations lead to an *s*-like bending of step edges on the sample surface. In spite of the step bending the topological antiferromagnetic order is strictly maintained. In some rare cases large scale images show a change of the spin-polarized part of the tunneling current. It is explained by the fourfold symmetry of the Cr(001) surface which leads to a 90° degeneracy and the formation of according domains.

DOI: 10.1103/PhysRevB.67.174411

PACS number(s): 75.70.Rf, 75.50.Ee, 68.37.Ef, 61.72.Ff

I. INTRODUCTION

Since the discovery of interesting magnetic effects such as giant magnetoresistance^{1,2} and interlayer exchange coupling³ and their rapid application in data storage devices the magnetism of Cr has attracted considerable interest. Bulk Cr exhibits a transversal spin-density wave (SDW) below the Néel transition temperature $T_N=311$ K and a longitudinal SDW below the spin-flip temperature $T_{SF}=121$ K. In particular, (001) terminated interfaces have been used in Fe/Cr multilayers.⁴ The magnetic properties of the Cr(001) surface have been studied theoretically and experimentally. Early experimental results were rather confusing since angle- and energy-resolved photoemission indicated that the Cr surface states are exchange split⁵ but no net magnetization was found by spin-resolved photoemission.⁶ This apparent inconsistency was explained by Blügel *et al.*⁷ who calculated that the magnetic moments of any atomically flat terrace couple parallel but—as a result of the antiferromagnetism of Cr—adjacent terraces are magnetized antiparallel. Since this model implies a close link between the surface topology and the magnetic structure the magnetic state of Cr(001) was called “topological antiferromagnetism.”

A direct experimental proof of the existence of topological antiferromagnetism is difficult. Since the magnetization direction alternates laterally and vertically with periodicities which are given by the average terrace width and the interlayer distance, respectively, the experimental method of choice must have a high lateral resolution and a high surface sensitivity. Both conditions are fulfilled by scanning tunneling microscopy (STM). As has been shown by Wiesendanger *et al.*⁸ STM can be made sensitive to the spin of the tunneling electrons by using a magnetic tip providing experimental evidence for the correctness of the theoretical predictions. Recently, the topological antiferromagnetic spin structure of Cr(001) was imaged by spin-polarized scanning tunneling spectroscopy that allows a clear separation between topo-

graphic, electronic, and magnetic contributions to the measured signal.^{9,10}

Here we report on the influence of screw and step dislocations, which are regularly found even in single-crystalline samples,¹¹ on the magnetic structure of the Cr(001) surface. After a brief description of the experimental setup, tip, and sample preparation procedures, and the contrast mechanism of spin-polarized scanning tunneling spectroscopy in Sec. II, we will present images of the undisturbed “topological antiferromagnetism” of Cr(001) as found on defect-free surfaces (Sec. III A). In Sec. III B we will introduce the two elementary defects, i.e., screw and step dislocations, and discuss how they change the spin structure of Cr(001). We will show in Sec. III C that two degenerated domains, which are rotated by 90°, can be found on the fourfold-symmetric Cr(001) surface. The results are summarized in Sec. IV.

II. EXPERIMENT

The experiments were performed in an ultrahigh vacuum (UHV) system with two separate chambers: a preparation chamber for the tip and sample treatment and an analysis chamber for sample surface characterization by means of low-energy electron diffraction (LEED) and Auger electron spectroscopy (AES). Furthermore, a satellite of the analysis chamber contains a combined atomic force and scanning tunneling microscope (AFM/STM) which has a maximum scan range of $6\ \mu\text{m}\times 6\ \mu\text{m}$ and which is operated at room temperature (RT). The base pressure in both chambers is in the low 10^{-11} torr range. As already described in previous publications^{9,10} the Cr(001) single crystal was cleaned by prolonged cycles of Ar⁺-ion etching at elevated temperatures ($T\leq 1100$ K) and subsequent annealing for 20–30 min at $T=1150$ K. However, compared to earlier results the amount of residual impurities could be reduced significantly by using an Ar⁺-ion gun with a mass filter (Wien filter). Eventually, the Cr(001) surface contains less than 2% of carbon (C). All other elements, as, e.g., O, S, and N, are below

the AES sensitivity limit of $\leq 1\%$. The cleanliness of the surface is corroborated by the existence of a d_{z^2} -like surface state close to the Fermi level E_F which showed up as a distinct peak in scanning tunneling spectroscopy (STS) measurements^{9,10} and which is characteristic for clean bcc(001) surfaces.¹²

We used polycrystalline W tips which were electrochemically etched *ex situ* and cleaned *in vacuo* by a high-temperature flash at $T \geq 2200$ K. Spin-resolved studies were carried out by using *in situ* prepared Fe-coated W tips. Details of the tip preparation procedure are described in Ref. 13. We know from previous experiments, which partly have been performed in an external magnetic field, that Fe-coated W tips are preferentially magnetized perpendicular to the tip axis,^{13,14} i.e., parallel to the sample's surface plane. The tunneling spectra were measured by adding a modulation voltage $U_{\text{mod}} = 15$ mV_{rms} to the applied sample bias U and recording the dI/dU signal by lock-in technique.

The above mentioned d_{z^2} -like surface state is well suited for mapping the magnetic domain structure of Cr(001) as it is the minority-spin part of an exchange split d band and exhibits a spin polarization of about 20%.^{8,9} By coating the W tips with Fe we produce magnetic tips with an intrinsic spin polarization. If both electrodes are spin polarized the tunneling current can be described by¹⁵

$$I_{\text{sp}}(\vec{r}, U_0) = I_0 [1 + P_s P_t \cos(\vec{M}_s, \vec{M}_t)], \quad (1)$$

where $I_0 = I_0(\vec{r}, U_0)$ is the non-spin-polarized part of the tunneling current and P_t and P_s are the spin polarization of the tip and the sample, respectively. For an electronically homogeneous surface I_0 and P_s are independent of the location (\vec{r}). Therefore it is qualitatively clear that any lateral variation of the tunneling current or its derivative dI/dU is due to a change of the $\cos(\vec{M}_s, \vec{M}_t)$ term, i.e., it contains information on the local orientation of the sample magnetization direction \vec{M}_s relative to the tip magnetization \vec{M}_t . However, in contrast to the Cr(001) surface with well-defined structural and spin dependent electronic properties the shape of the cluster at the tip apex cannot be controlled in our experimental setup. Since the atomic structure of this cluster determines its (spin dependent) electronic properties and since P_t , just as P_s , is a bias voltage dependent quantity, the bias voltage at which the product $P_s \cdot P_t$ becomes maximal cannot be predicted and varies between different experimental runs.

At RT, i.e., about 20 K below the Néel temperature of bulk Cr of $T_N = 311$ K, different relative tip-sample magnetization directions (parallel versus antiparallel) typically result in a change of the dI/dU signal by $\leq 12\%$. This result may be surprising, especially in view of the relatively high reduced temperature $T/T_N \approx 0.94$. We would like to emphasize, however, that in the Stoner picture the magnetization $M(T)$ behaves like $M(T)/M(0) = (1 - T/T_N)^\beta$, where β is the critical exponent. Assuming $\beta = 0.33$ results in $M(293 \text{ K})/M(0) \approx 0.4$, i.e., at $T = 293$ K the sample still possesses 40% of its zero-temperature magnetization.

All "topographic" STM images shown below were measured in the constant-current mode of operation. The STM

data have been plane-fitted on atomically flat terraces to correct for the tilt of the sample. In order to enhance the contrast we mixed the tip height z and its derivative with respect to the fast scan direction x , dz/dx . This image processing suggests to the spectator a topography which is illuminated by an invisible light source from the left.

III. RESULTS AND DISCUSSION

A. Defect-free surfaces

Figure 1(a) shows the topography of a clean Cr(001) surface. Eight terraces can be recognized which descend from the upper right to the lower left edge of the image. The section in the lower panel of Fig. 1(a) has been drawn along the line in the image. It reveals that adjacent terraces are separated by monatomic steps of 1.45 Å height. This terrace and step structure which is found on any real surface is the result of a slight miscut (locally about 0.04° , averaged over the whole sample surface approximately 0.15°) with respect to the ideal (001) surface. Apart from these step edges the frame of view is free of any defect. Figure 1(b) shows the simultaneously acquired map of the differential conductivity dI/dU as measured with a Fe-coated tungsten tip. Obviously, the strength of the dI/dU signal abruptly changes between two discrete levels at any step edges which separates adjacent atomically flat terraces. This is a result of spin-polarized tunneling between the magnetic sample and the magnetic tip. Figure 1(b) nicely confirms the model of "topological antiferromagnetism" as proposed by Blügel *et al.*⁷

B. Dislocations

To our experience structural defects are regularly found even on well-prepared Cr(001) surfaces. These defects may be complex, but they can always be reduced to a superposition of the two elementary defects, i.e., screw and step dislocations as schematically represented in Figs. 2(a) and (b), respectively. Both, screw as well as step dislocations are defined by the so-called Burgers vector \vec{b} which describes the line along which one half of the crystal is displaced. In any case the crystal is cut along the plane \overline{ABCD} . To create a screw dislocation all lattice sites on the left side of plane \overline{ABCD} are shifted by half of the cubic lattice constant along \overline{AD} while the right side is kept fixed. The Burgers vector \vec{b} of a screw dislocation is pointing parallel to the dislocation line \overline{BC} . If the top plane of Fig. 2(a) is imaged an additional, semi-infinite step edge appears on the surface at point C. In contrast, a step dislocation [Fig. 2(b)] is formed by moving the lower left part of the crystal along \overline{AB} while the upper left part stays at place. Consequently, the Burgers vector \vec{b} of a step dislocation is perpendicular to the dislocation line \overline{BC} . Effectively, an additional semi-infinite plane (as indicated by the gray line) is inserted into the crystal. If the dislocation line \overline{BC} is located sufficiently close to the imaged surface [top plane of Fig. 2(b)] the resulting mechanical strain cannot relax and the surface buckles by half of the cubic lattice constant. As we will see in the following, both dislocations make the magnetic structure more complicated.

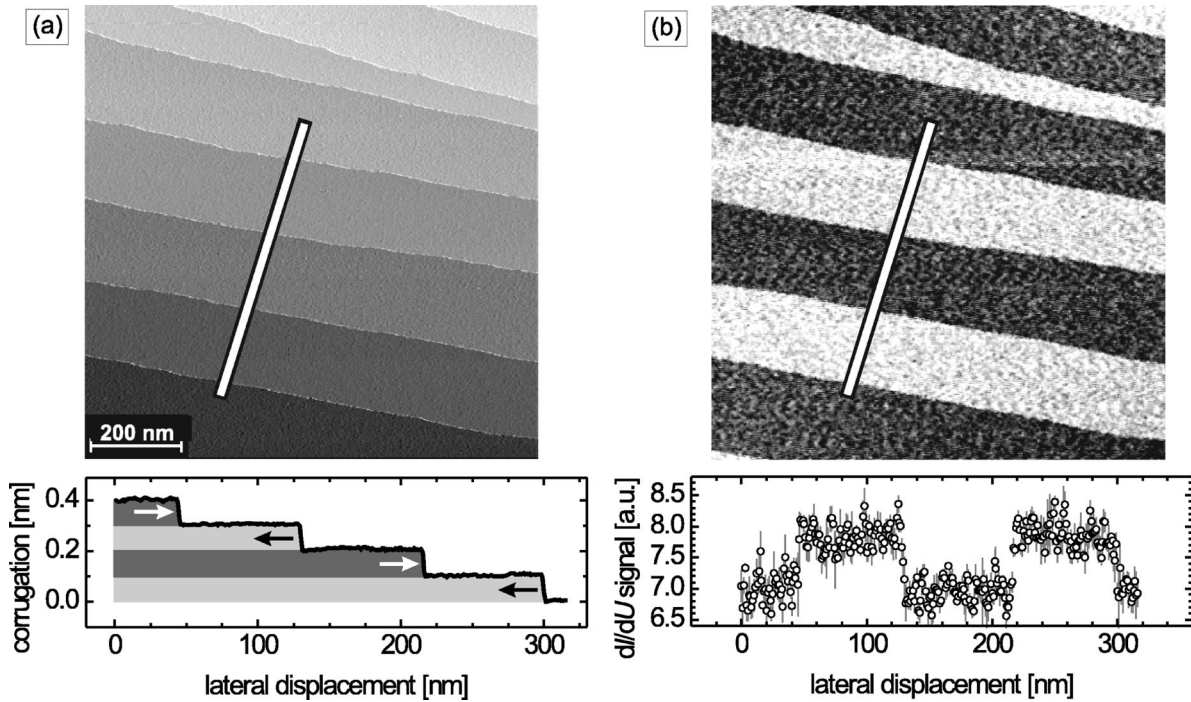


FIG. 1. (a) Topography and (b) spin-resolved map of the dI/dU signal of a clean and defect free Cr(001) surface as measured with a Fe-coated tip. The bottom panels show averaged sections drawn along the line. Adjacent terraces are separated by steps of monatomic height. The measurement parameters are $U = -150$ mV and $I = 0.7$ nA.

1. Screw dislocations

Figure 3(a) shows the topography of a surface area of the Cr(001) single crystal with two screw dislocations which are marked by arrows. Each screw dislocation leads to the formation of a semi-infinite step edge which starts at the respective point of interception of the dislocation line with the Cr(001) surface plane. The two step edges propagate in opposite directions. Our results indicate that step edges which are caused by screw dislocations are oriented almost parallel towards other step edges. Thereby, the crossing of different step edges is avoided.

Obviously, the resulting terrace-and-step structure of Fig. 3(a) cannot exhibit a perfect topological antiferromagnetic order as shown in Fig. 1. The simultaneously recorded dI/dU map [Fig. 3(b)] reveals that the topological antiferromagnetic order remains unchanged in the upper right and lower left corner of the image. The order is frustrated, however, between the two screw dislocations where a domain wall is formed. We have determined the domain-wall width by drawing line sections along the lines (i) and (ii) in Fig. 3(b). The result is plotted in Fig. 3(c). Both domain-wall profiles exhibit a gradual and slightly asymmetric transition region with a width of 100–200 nm. The asymmetric shape of the domain-wall profile indicates that tip and sample magnetization are not collinear but canted.

A quantitative analysis can be performed on the basis of continuum micromagnetic theory.¹⁶ We have fitted the measured data with a standard domain-wall profile,

$$y(x) = y_0 + y_{sp} \cdot \cos(\arccos\{\tanh[(x-x_0)/(w/2)]\} + \phi), \quad (2)$$

where $y(x)$ is the dI/dU signal measured at position x , x_0 is the position of the domain-wall, w the domain wall width, y_0 and y_{sp} are the non-spin-polarized and spin-polarized part of the dI/dU signal. ϕ is the angle between the tip and sample magnetization. The best fits for domain-wall profiles were achieved with $\phi = 30^\circ$ leading to a width of $w_i = 145 \pm 4$ nm and $w_{ii} = 109 \pm 3$ nm. The width of wall (i) is in good agreement with former results which showed a domain-wall width of 120–170 nm.^{9,10} As we will see below the width of the wall (ii) is reduced because of its close proximity to the screw dislocation.

Although Fe-coated W tips are usually magnetized perpendicular to the tip axis which makes them sensitive to the in-plane component of the sample magnetization a slight out-of-plane component cannot be excluded. Therefore on the basis of the experimental data shown in Fig. 3(b) it is not possible to determine whether the observed domain walls are Bloch or Néel walls, i.e., whether the magnetization in the center of the wall is parallel or perpendicular to the wall plane, respectively. It is well known that domain walls in ferromagnetic bulk materials like Fe prefer the Bloch type because this avoids any stray field energy due to “magnetic charges.”¹⁶ At the surface, however, the magnetization of a Bloch wall would produce a magnetic stray field. Therefore the Bloch wall of a ferromagnetic sample is capped with a Néel-type structure.^{17,18} In contrast, the stray field energy plays no role in an antiferromagnet like Cr, since adjacent magnetic moments cancel each other, and other parameters like, e.g., the surface anisotropy, determine the character of the wall. To our opinion previous experiments indicate that domain walls found on Cr(001) are Néel walls: Firstly, it was

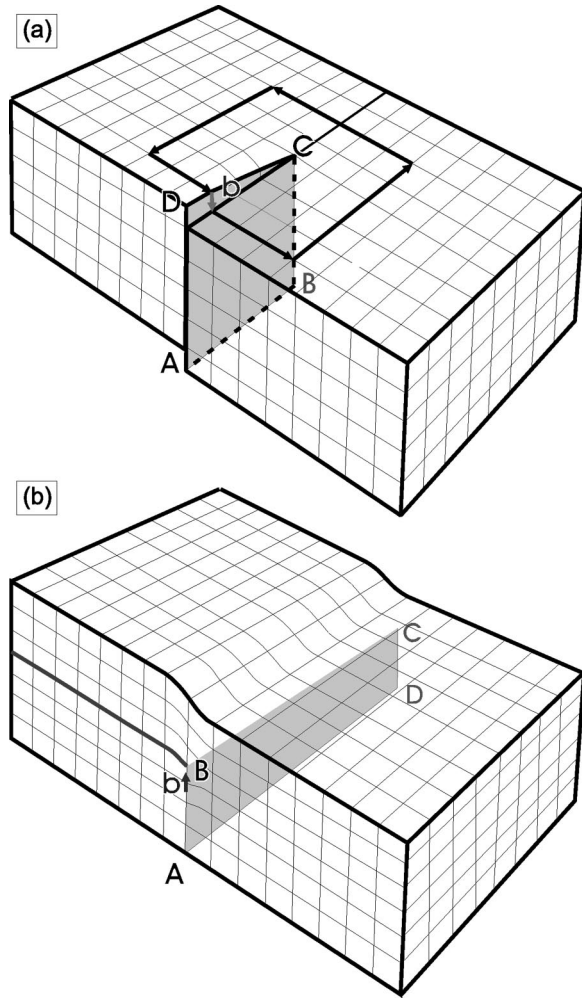


FIG. 2. Schematic representation of (a) a screw and (b) a step dislocation.

shown that both the charge-density wave (CDW) and the spin-density wave (SDW) preferentially propagate perpendicular to the surface plane in the near surface region. For example, x-ray scattering¹⁹ on Cr(001) and scanning tunneling spectroscopy²⁰ on Cr(001) reveal that the particular domain with the propagation vector within the sample surface is strongly damped. As corroborated by spin-polarized (SP)-STM,¹⁰ this leads to an in-plane orientation of the surface magnetic moments for the transversal SDW, i.e., at $T_{SF} < T < T_N$. Furthermore, large lateral-scale SP-STM images revealed that the contrast between adjacent terraces does not change for different surface sites indicating that the SDW always pins with an antinode at the surface.¹⁰ In other words, the SDW adopts a position such that a maximum in-plane value of the magnetic moment is obtained all over the Cr(001) surface, which is consistent with the predicted enhanced magnetic moment at the Cr surface.^{7,21} Therefore, it can be expected that the magnetization within the domain wall remains in-plane which then results in a Néel wall. A definite proof requires a tip with an out-of-plane sensitivity.

Up to now any domain wall we have observed was caused by a screw dislocations. As mentioned above the averaged domain-wall width as measured far away from the screw

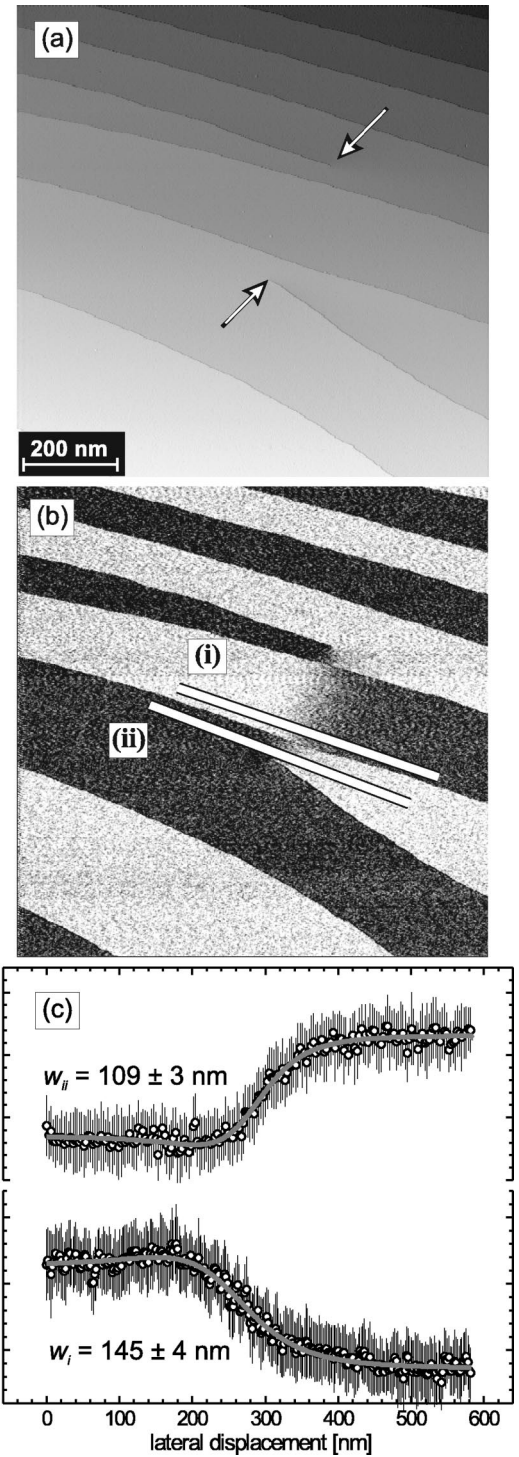


FIG. 3. (a) Topography and (b) magnetic dI/dU signal of a Cr(001) surface with two screw dislocations (measurement parameters: $U = -150$ mV and $I = 0.7$ nA). The magnetic frustration leads to the formation of a domain wall between the dislocation. (c) Line sections drawn across the domain wall on two adjacent terraces along the lines in (b). The fit of the domain-wall profiles result in wall width of 145 and 110 nm.

dislocation on a stepped Cr(001) surface amounts to 120–170 nm. In analogy to ferromagnetic domain walls this value is determined by intrinsic material parameters, i.e., the strength of the exchange coupling and the magnetocrystalline

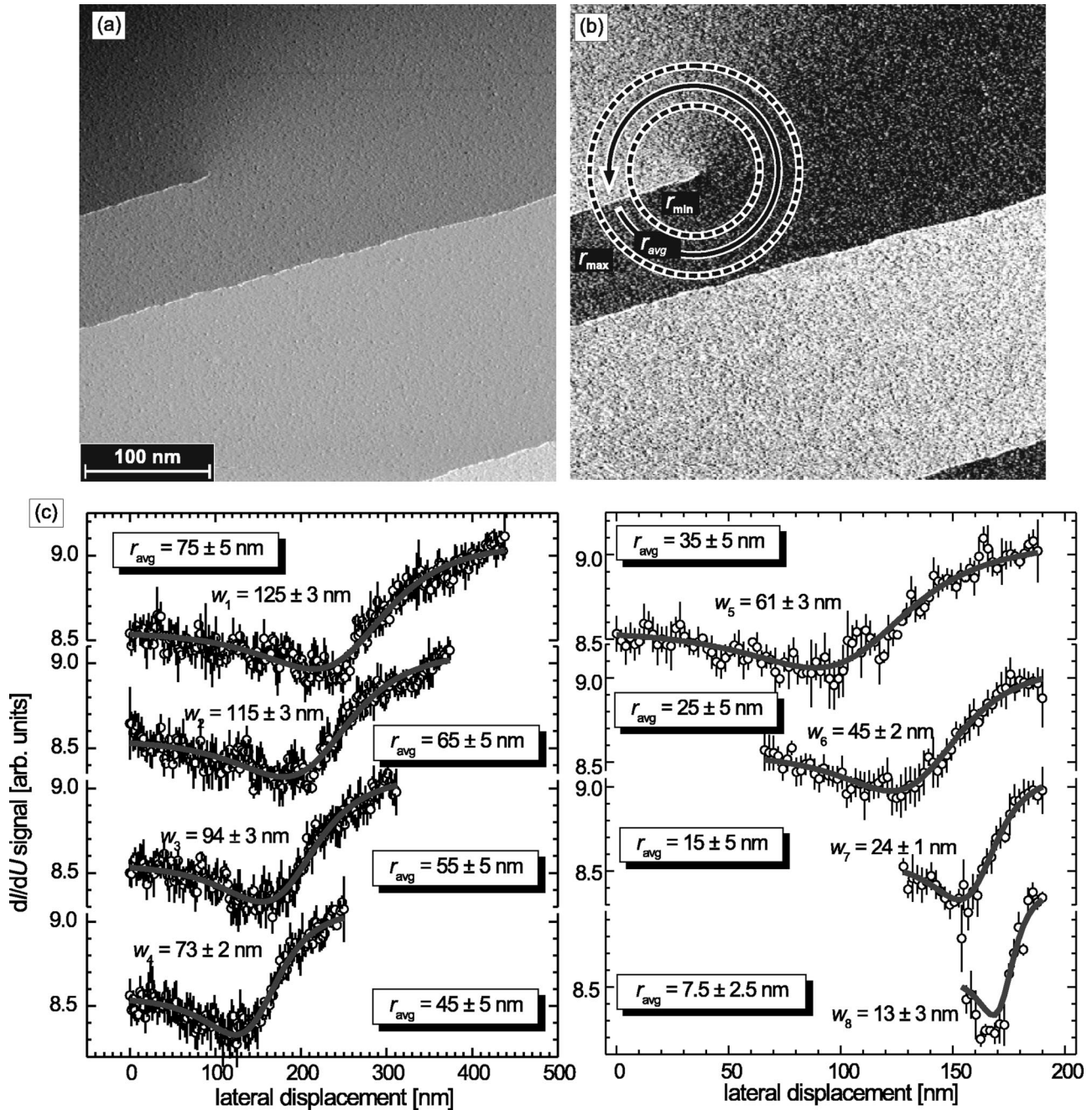


FIG. 4. (a) Topography and (b) magnetic dI/dU signal of a Cr(001) surface with a single screw dislocation (measurement parameters: $U = -43$ mV and $I = 0.22$ nA). The magnetic frustration leads to the formation of a domain wall between the dislocation. (c) Circular sections drawn at different radii around the center of the screw dislocation.

anisotropy. Obviously, the domain-wall width cannot remain unchanged very close to the screw dislocation where the circumference becomes comparable with or smaller than the intrinsic domain-wall width.

We have experimentally studied the dependence of the domain-wall width on the distance from the screw dislocation at the location of the Cr(001) surface which is shown in Fig. 4(a). Approximately 100 nm from the next step edge a single screw dislocation can be recognized in the upper left corner of the image. The magnetic dI/dU map of Fig. 4(b) reveals that this screw dislocation is the starting point of a

domain wall which propagates towards the upper side of the image. Starting at the tail of the arrow (zero lateral displacement) we have drawn eight circular line sections counter-clockwise around the screw dislocation at different radii r_{avg} from 75 nm down to 7.5 nm. The data are plotted in Fig. 4(c). In order to improve the signal-to-noise ratio the data have been averaged between r_{min} and r_{max} . Apart from the shortest circular section ($r_{\text{avg}} = 7.5 \pm 2.5$ nm) the averaging was performed over $r_{\text{avg}} \pm 5$ nm by radially projecting the measured data onto the minimal radius r_{min} . Again, the domain-wall profiles were fitted with Eq. (2). However, the

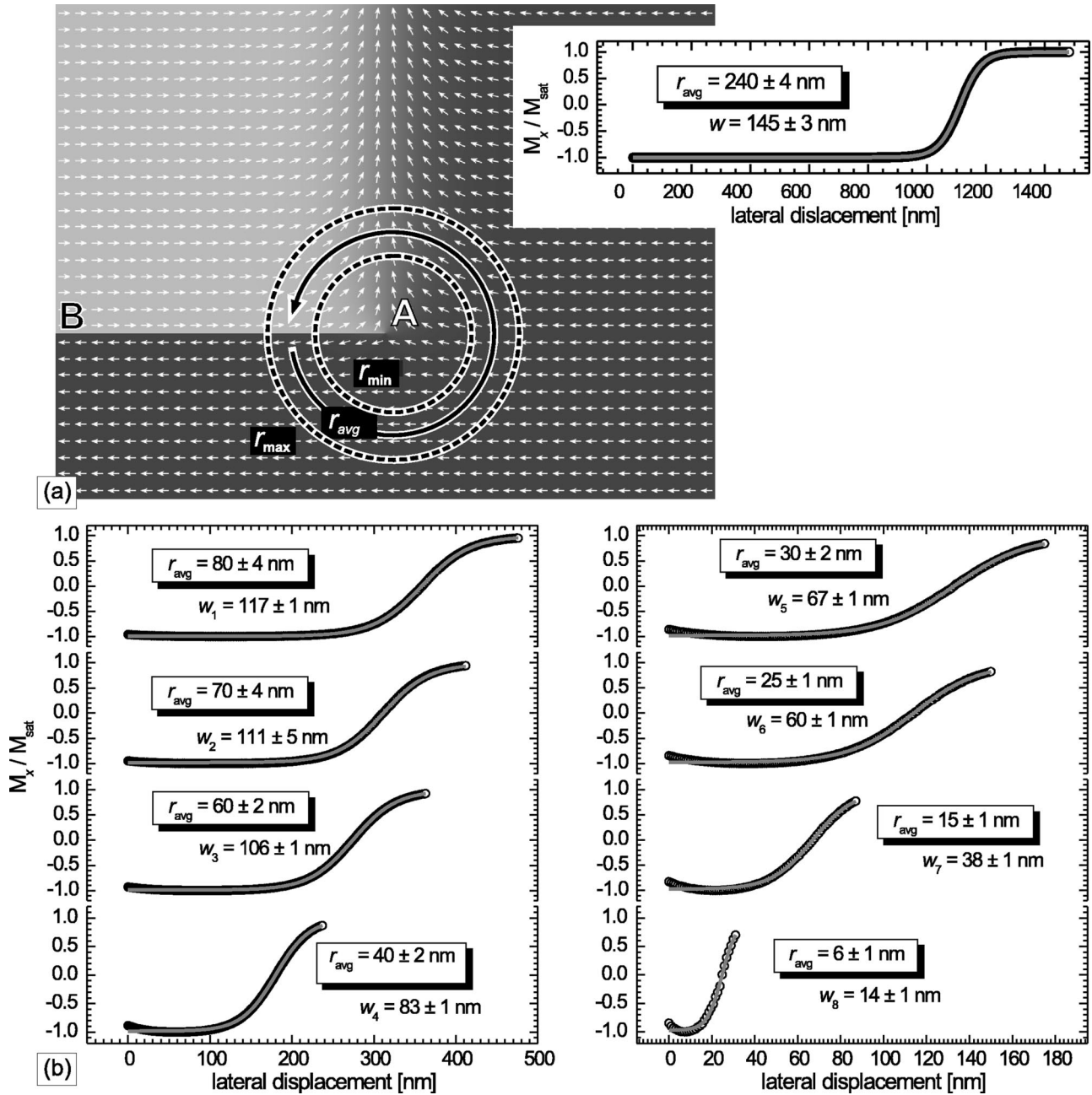


FIG. 5. (a) Calculated spin structure (Ref. 22) of a screw dislocation (1000×750 nm). The inset shows a circular section around the screw dislocation of the x component of the magnetization measured at an average radius $r_{\text{avg}} = 240$ nm. This and larger radii result in domain-wall widths w being consistent with an infinite domain wall. (b) Circular sections of the calculated spin structure (\circ) drawn at different radii around the center of the screw dislocation. Each circular section was fitted with Eq. (2) (gray line).

fitting procedure has been performed in two steps. In the first step, we fitted the eight domain walls independently, i.e., with individual fitting parameters y_0 , y_{sp} , and ϕ . Since the data of the eight domain-wall profiles were taken from a single data set [Fig. 4(b)], which has been measured with the same tip, y_0 , y_{sp} , and ϕ should be identical for all of them. Indeed, a very small scatter was found ($y_0 = 8.81 \pm 0.02$, $y_{\text{sp}} = 0.48 \pm 0.02$, and $\phi = -57 \pm 2^\circ$). In a second step, the domain walls were again fitted but now y_0 , y_{sp} , and ϕ were kept fixed at the average values. The results are shown as gray lines in [Fig. 4(c)]. Except for the smallest average ra-

dius ($r_{\text{avg}} = 7.5 \pm 2.5$ nm) we find an excellent agreement with the experimental data. At an average radius $r_{\text{avg}} = 75$ nm the domain-wall width is $w_1 = 125 \pm 3$ nm being in close agreement with the intrinsic domain-wall width of Cr(001) as determined far away from screw dislocations. This may not be surprising as the circumference amounts to 471 nm which is much larger than the intrinsic domain-wall width. However, as soon as r_{avg} is reduced below 60 nm a significant reduction of the domain-wall width can be observed although the circumference still exceeds the intrinsic domain-wall width: The following values of the domain-wall

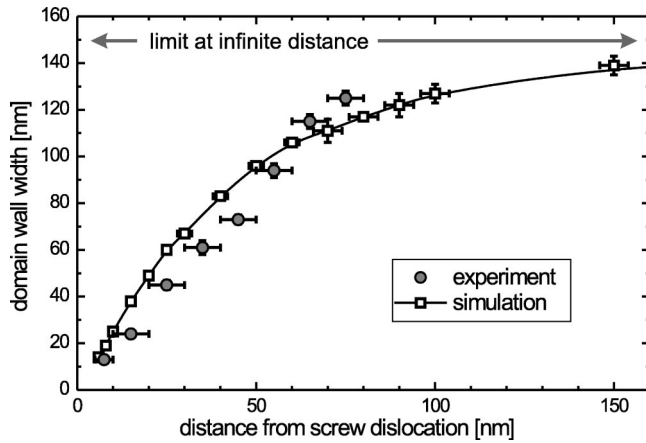


FIG. 6. Plot of the experimentally determined and micromagnetically simulated domain-wall width in a layered antiferromagnet in dependence on the distance from a screw dislocation. The interconnecting line between the data points serves as a guide for the eye only.

width have been found (circumferences in the brackets): $w_1 = 125 \pm 3$ nm (471 nm), $w_2 = 115 \pm 3$ nm (408 nm), $w_3 = 94 \pm 3$ nm (346 nm), $w_4 = 73 \pm 2$ nm (283 nm), $w_5 = 61 \pm 2$ nm (220 nm), $w_6 = 45 \pm 2$ nm (157 nm), $w_7 = 24 \pm 1$ nm (94 nm), and $w_8 = 13 \pm 3$ nm (47 nm). The results clearly show that the domain-wall width is always considerably narrower than the circumference of the cross section.

We have simulated the spin structure which is formed around a screw dislocation by performing micromagnetic calculations.²² The magnetic frustration as produced by a screw dislocation was generated by a negative exchange coupling along the line AB in Fig. 5(a) while keeping the exchange coupling positive elsewhere. The sample has lateral dimensions of $1000 \text{ nm} \times 750 \text{ nm}$ and a height of 2 nm. It was discretized into cells of $1 \text{ nm} \times 1 \text{ nm} \times 2 \text{ nm}$. According to the relationship $w = 2\sqrt{A/k}$ the domain-wall width w is one-to-one determined by the ratio A/k , where A is the so-called exchange stiffness and k is the effective anisotropy energy density. On the basis of the measured Cr domain-wall

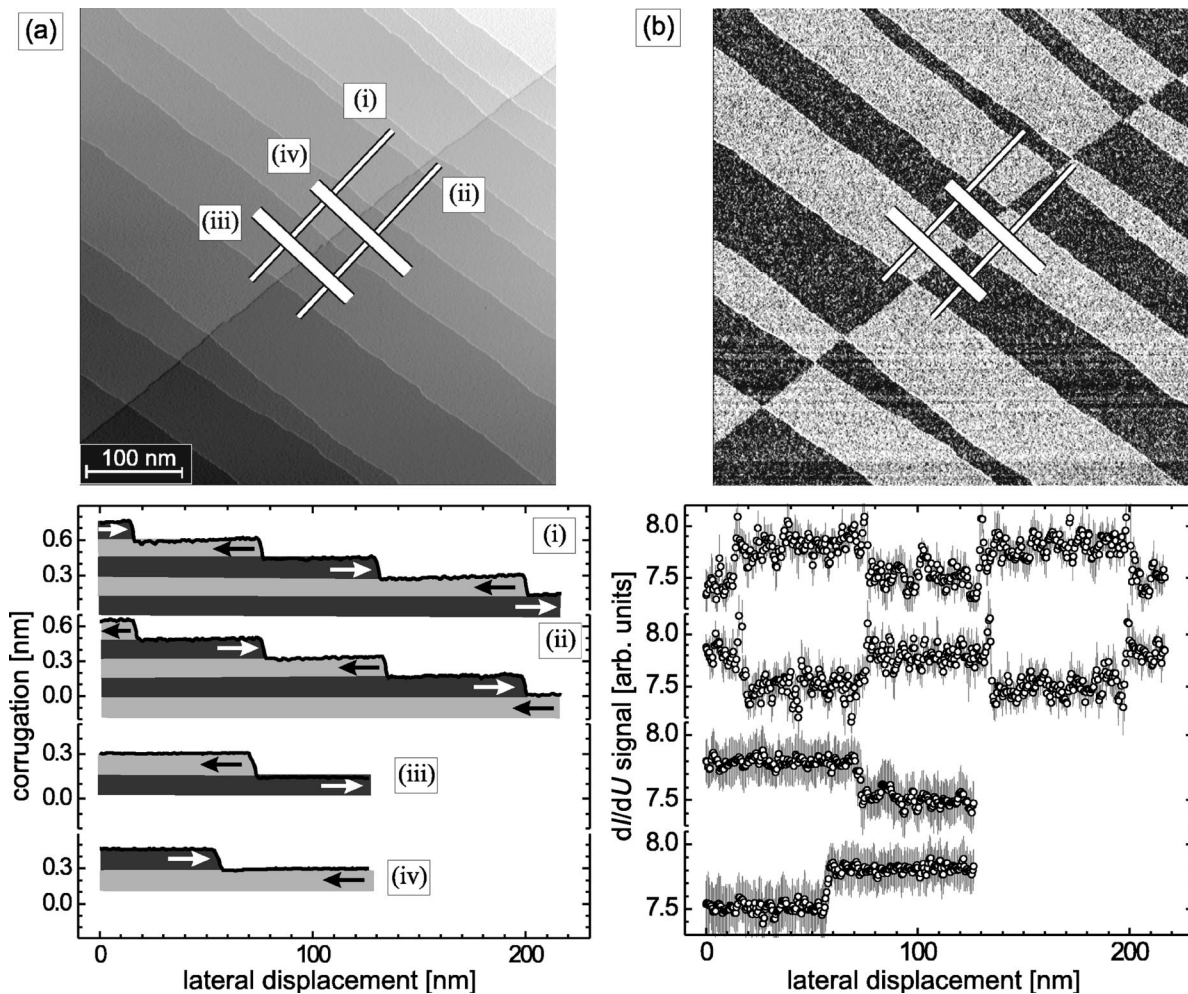


FIG. 7. (a) Topography and (b) map of the magnetic dI/dU signal of a Cr(001) surface with a step dislocation (measurement parameters: $U = -130$ mV and $I = 0.5$ nA). The bottom panels show averaged sections drawn along the lines (i)–(iv). The topological antiferromagnetic order of the surface is not distorted by the step dislocation.

width $w_{Cr}=150$ nm we can deduce that $A_{Cr}/k_{Cr}=5.625 \times 10^{-15}$ m². For instance, we may assume that $A_{Cr}=1 \times 10^{-11}$ J/m and $k_{Cr}=1.77 \times 10^3$ J/m³. We believe that in consideration of the fact that the ‘‘Stoner parameter’’ I of Cr, $I_{Cr}=0.58\text{--}0.68$ eV,^{23–25} is considerably smaller than $I_{Fe}=0.88$ eV,²⁶ this assumption for A_{Cr} is justified. Since the magnetic moments of adjacent atoms in antiferromagnets compensate each other Cr produces no stray field. Therefore it is not necessary to consider any demagnetizing field.

Our calculations showed that a magnetocrystalline anisotropy with fourfold symmetry, which may be expected on the (001) surface of a cubic material like Cr, always leads to the formation of two separate 90° domain walls around a screw dislocation. A similar behavior is also known from cubic ferromagnetic materials where—in the absence of uniaxial contributions to the anisotropy—a 180° domain wall tends to split into two 90° domain walls.¹⁶ This is in contrast to our experimental findings which clearly show a single 180° domain wall [cf. Fig. 4(b)]. In order to reproduce this result in the simulations we had to assume an uniaxial effective anisotropy. We speculate that—similar to cubic ferromagnetic materials—the uniaxial effective anisotropy is caused by a magnetostrictive self-energy.¹⁶ Since the domain wall profile exhibits only one point of inflection we can conclude that the ratio of the magnetostrictive and the magnetocrystalline anisotropy energy density $\kappa=K_{ms}/K_{mc} \geq -0.5$ (Ref. 16, p. 227ff). For a rough estimation we may assume for a moment that $k_{Cr}=1.77 \times 10^3$ J/m³ is dominated by magnetostrictive contributions. With $K_{ms}=\frac{9}{2}C_2\lambda_{100}^2$,¹⁶ where $C_2 \approx 1.4 \times 10^{11}$ N/m³ is the shear modulus of Cr, we can deduce $\lambda_{100} \approx 10^{-4}\text{--}10^{-5}$, which according to Hubert and Schäfer (Ref. 16, p. 134) is a rather typical value for magnetostriction.

The inset of Fig. 5(a) reveals that the chosen material parameters lead to a domain-wall width that is consistent with an infinite wall as long as a circular line section with a sufficiently large average radius ($r_{avg} \geq 240$ nm) is drawn around the screw dislocation. In some respects the spin structure around the screw dislocation shown in Fig. 5(a) resembles the magnetic configuration as found in small ferromagnetic islands, e.g., circular dots of permalloy with submicrometer size^{27,28} or small Fe islands on W(110).²⁹ These ferromagnetic particles minimize their stray field energy by the formation of a magnetic vortex where the magnetization continuously curls around the particle center. For topological reasons the magnetization in the vortex core, which is about 10 nm wide, must be orientated perpendicular to the surface. By using SP-STM Wachowiak *et al.*²⁹ recently proved that the size and the shape of the vortex core is governed by only two material parameters, i.e., the exchange stiffness and the saturation magnetization which determines the stray field energy. There exist, however, two differences between the spin frustration in an antiferromagnet around a screw dislocation and the spin structure of a ferromagnetic vortex which are of great importance for the resulting spin structure: (i) In contrast to the ferromagnetic vortex the magnetization of which continuously rotates by 360° around the vortex core and which—as no other direction is left—must lead to an out-of-plane magnetization in the vortex core, the

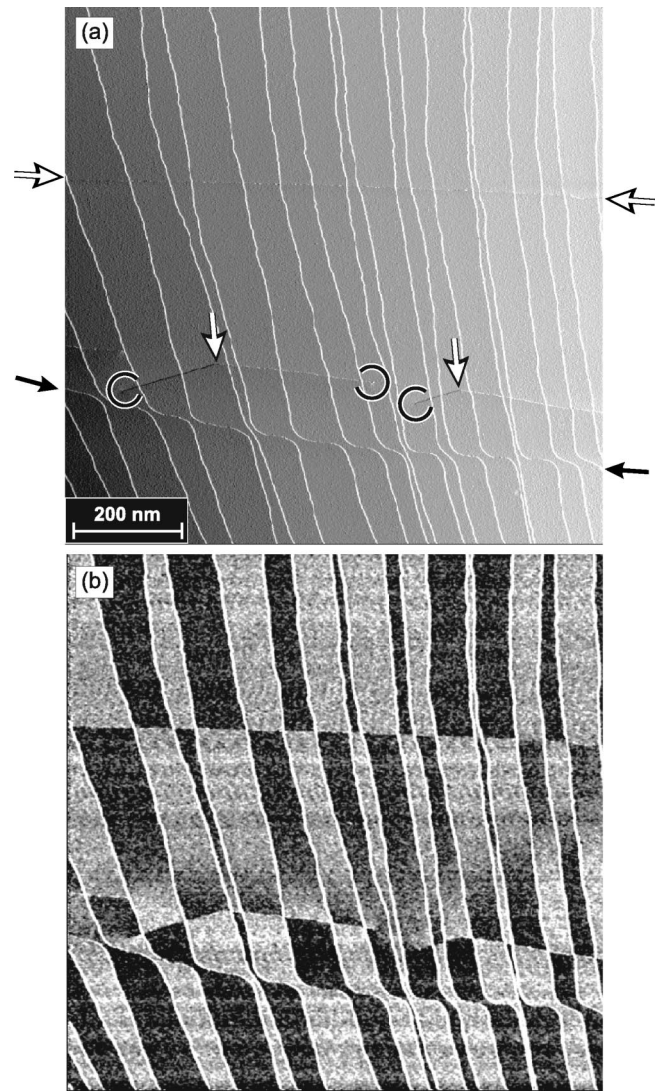


FIG. 8. (a) Topography and (b) map of the magnetic dI/dU signal of a Cr(001) surface with step and screw dislocations (measurement parameters: $U = -130$ mV and $I = 0.5$ nA).

intersection of the screw dislocation with the sample surface causes a change from negative and positive coupling constants (180°) along the line \overline{AB} and beyond point A, respectively. This frustration may be compensated by a rotation either through the out-of-plane or through the in-plane direction which is perpendicular to the magnetization direction far away from the screw dislocation. In other words, a perpendicular component is possible but not necessary. We believe that in the case of Cr(001) the surface anisotropy prefers an in-plane orientation. (ii) In contrast to a ferromagnetic vortex core the size and shape of which is governed by only two material parameters, i.e., the exchange stiffness and the saturation magnetization, the latter plays no role in an antiferromagnet and is to be replaced by the effective anisotropy.

In analogy to the previously presented experimental results [cf. Fig. 4(b)], eight circular line sections which were drawn at different average radii r_{avg} around the simulated screw dislocation (point A) are shown in Fig. 5(b). In order to quantify the domain-wall width each circular section was

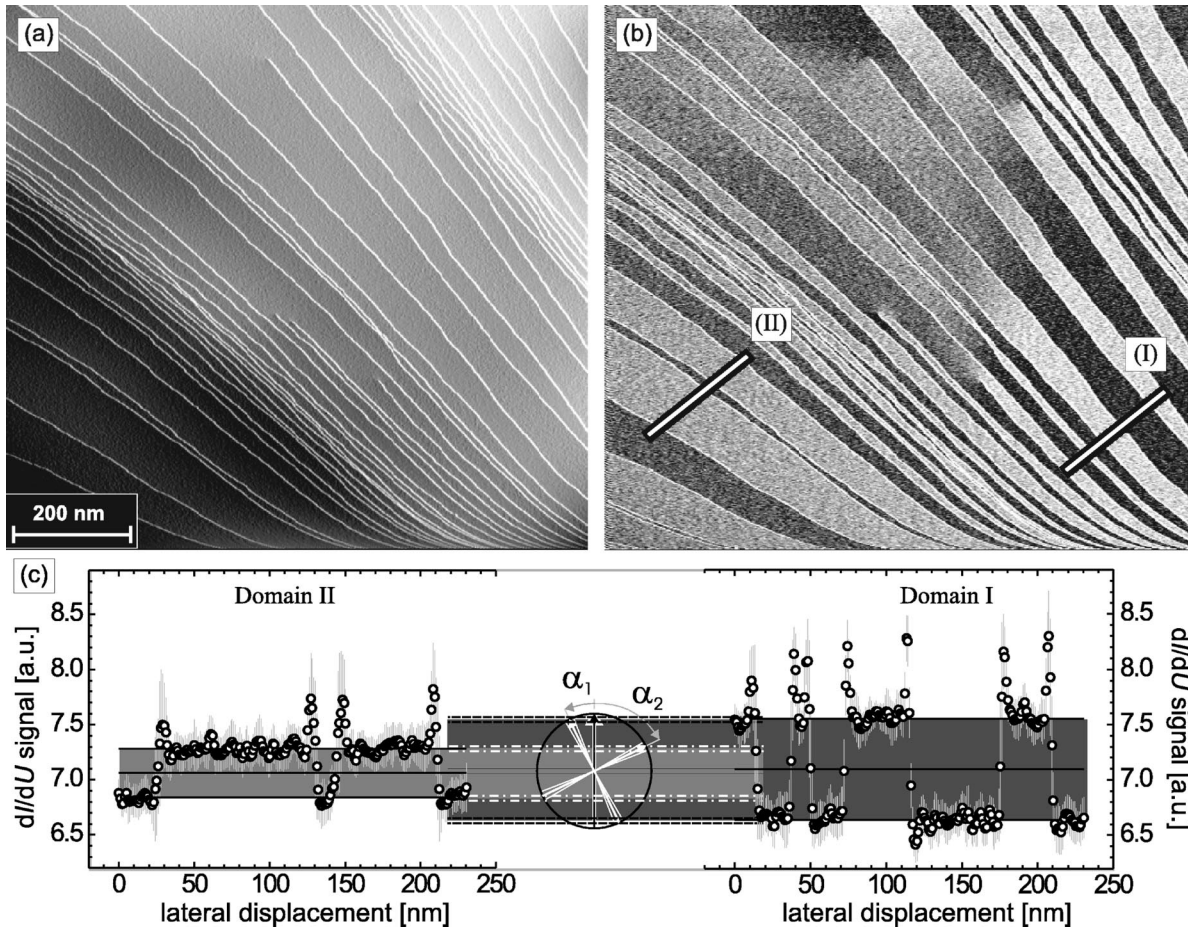


FIG. 9. Large scale images of the (a) topography and (b) magnetic dI/dU signal of a Cr(001) surface with multiple screw dislocations (measurement parameters: $U = -130$ mV and $I = 0.5$ nA). In (b) the magnetic contrast is much stronger on the right (I) than on the left side (II) of the image. The variation of the contrast is caused by two domains which are rotated by 90° towards each other and which are equivalent on Cr(001) with its fourfold symmetry. (c) An analysis of the line sections measured along the lines indicated in (b) allows a determination of the azimuth of the tip magnetization direction.

fitted with Eq. (2) (gray line). Experimental and theoretical results are summarized in Fig. 6. The excellent agreement between experimental and micromagnetically simulated data confirms that the shape of the spin structure around the screw dislocation in a layered antiferromagnet is determined by the exchange stiffness A and the effective anisotropy k . The small deviation at $20 \text{ nm} \leq r_{\text{avg}} \leq 50 \text{ nm}$ may be caused by the elastic deformation of the crystal lattice around the screw dislocation which has not been considered in the simulations.

2. Step dislocations

The second distortion of the crystal structure we want to discuss is a step dislocation. The first hint that step dislocations exist on Cr(001) surfaces was derived from the data shown in Fig. 7. The constant current “topography” image in Fig. 7(a) exhibits eleven normal step edges running from the upper left to the lower right corner. These step edges are crossed by another almost perpendicularly arranged step edge. We relate the latter step edge to a relaxed step dislocation. As a result of these crossing steps a double step exists at the point of intersection with kinks in either step edge. Probably, during the final annealing step the semi-infinite lattice

plane, which is inserted into the crystal [cf. dark line in Fig. 2(b)] and forms the step dislocation, has migrated to the surface leading to its annihilation. Line sections drawn along the rectangles in Figs. 7(a) and (b) are plotted in the lower panels. A comparison between a normal step [line sections (i) and (ii)] and the relaxed step dislocation [line sections (iii) and (iv)] reveals an identical step height of a 1.47 ± 0.03 nm being consistent with the Cr lattice constant. As evidenced by the magnetic dI/dU map in Fig. 7(b) every step edge—irrespective of its origin—leads to a reversal of the surface magnetization, i.e., the topological antiferromagnetic order is maintained.

The topography and the magnetic dI/dU map of Cr(001) as measured on a larger lateral scale is shown in Figs. 8(a) and (b), respectively. Again, a relaxed step dislocation can be recognized in the upper part of the images. Since this step edge is almost parallel with the fast scan direction it is only weakly visible between the white arrows in the topographic image [Fig. 8(a)]. However, the resulting distortion of the surface magnetic structure is clearly observable in the magnetic dI/dU map [Fig. 8(b)]. In addition, a noncontinuous step edge is found between the black arrows in Fig. 8(a). At

this location each individual normal step edge fulfills an *s*-like curvature resulting in a lateral offset which is equivalent to one terrace width. Effectively, the surface level in the lower part of the image is lowered by one half of the Cr lattice constant. We believe that this structural feature is caused by a relaxed step dislocation, but in contrast to the step dislocation shown in Fig. 7 the step edges are smoothed, possibly to remove energetically unfavorable kink sites. In spite of this structural defect the surface magnetic structure of Cr(001) strictly maintains its topological antiferromagnetic order as can be seen in Fig. 8(b). This result confirms our earlier finding that the antinode of the Cr spin-density wave is strongly pinned to the (001) surface.¹⁰ More complicated structures are found in the middle part of Fig. 8 where two obtuse angled ($\approx 155^\circ$), about 500-nm-long step dislocations are visible. A screw dislocation (circle) can be found at each end of a step dislocation.

C. Domain issues

As bcc Cr has a fourfold symmetry two degenerate domains of the topological antiferromagnetic order with an orientation perpendicular to each other are possible. Since SP-STM is sensitive to the projection of the surface magnetization onto the tip magnetization [cf. Eq. (1)] such a domain formation would generally lead to two different dark/bright intensities. Only the unlikely case that the tip magnetization is rotated by 45° with respect to *both* domains would result in the same signal strength. Previous SP-STM measurements^{9,10} never showed such domains. The explanation could be a single domain state of the entire sample or domains being much larger than the scan range. Indeed, recent magnetic x-ray-diffraction microscopy measurements by Evens *et al.*³⁰ which have been performed around T_{SF} revealed domain sizes from tens to hundreds of μm .

Meanwhile, in some rare cases we have also found evidence for the existence of degenerate domains on clean Cr(001). For example, the constant current image of Fig. 9(a) shows the topography of a particular location of the Cr single crystal with numerous steps and screw dislocations. Two different contrast levels can be distinguished in the left and right side of the dI/dU map [Fig. 9(b)]. We have analyzed the signal strength in both regions by drawing two line sections. The result is plotted in Fig. 9(c). In fact, the respective amplitudes in domains I and II, $A_I=0.91$ a.u. (arb. units) and

$A_{II}=0.44$ a.u., differ significantly. On the basis of Eq. (1) we can calculate the relative orientation between the tip magnetization and the magnetization of the two domains which is given by the relations

$$\tan \alpha_1 = \frac{A_{II}}{A_I} \quad (3)$$

and

$$\alpha_1 + \alpha_2 = 90^\circ. \quad (4)$$

We obtained $\alpha_1 = 25.8 \pm 4.5^\circ$ and $\alpha_2 = 64.2 \pm 4.6^\circ$. The result is schematically represented in the middle part of Fig. 9(c) with the tip as a black upright arrow and the orientation of the sample domains as white arrows and error margins.

IV. SUMMARY

In summary, we have imaged the surface spin structure of Cr(001) and the effect of screw and step dislocations on it. Screw dislocations were found to cause domain walls. At sufficiently large distance from the screw dislocation (>60 nm) the domain-wall width amounts to 120–170 nm. At smaller distances narrower domain walls were found. The spin structure around a screw dislocation in Cr(001) was simulated by micromagnetic calculations using an uniaxial effective anisotropy which is probably caused by a magnetostrictive self-energy. An excellent agreement between the measured and the simulated data was found indicating that the width and the shape of the spin frustration around the dislocation is determined by two material parameters, i.e., the exchange stiffness and the effective anisotropy. In the case of step dislocations, irrespective of whether they are straight or exhibit an *s*-like bending, the topological antiferromagnetic order is strictly maintained. In some rare cases large scale images show a change of the spin-polarized part of the tunneling current which is probably caused by the fourfold symmetry of the Cr(001) surface.

ACKNOWLEDGMENTS

Financial support from the BMBF (Grant No. 13N7647) and from the DFG (Graduiertenkolleg “Nanostrukturierte Festkörper”) is gratefully acknowledged. We thank G. Bihlmayer (FZ Jülich) for helpful discussions.

¹G. Binasch, P. Grünberg, F. Saurenbach, and W. Zinn, Phys. Rev. B **39**, 4828 (1989).

²M. N. Baibich, J. M. Broto, A. Fert, F. N. V. Dau, F. Petroff, P. Eitenne, G. Creuzet, A. Friederich, and J. Chazelas, Phys. Rev. Lett. **61**, 2472 (1988).

³P. Grünberg, Prog. Surf. Sci. **18**, 1 (1985).

⁴H. Zabel, J. Phys.: Condens. Matter **11**, 9303 (1999).

⁵L. E. Klebanoff, S. W. Robey, G. Liu, and D. A. Shirley, Phys. Rev. B **30**, 1048 (1984).

⁶F. Meier, D. Pescia, and T. Schriber, Phys. Rev. Lett. **48**, 645 (1982).

⁷S. Blügel, D. Pescia, and P. H. Dederichs, Phys. Rev. B **39**, 1392 (1989).

⁸R. Wiesendanger, H. J. Güntherodt, G. Güntherodt, R. J. Gambino, and R. Ruf, Phys. Rev. Lett. **65**, 247 (1990).

⁹M. Kleiber, M. Bode, R. Ravlić, and R. Wiesendanger, Phys. Rev. Lett. **85**, 4606 (2000).

¹⁰M. Kleiber, M. Bode, R. Ravlić, N. Tezuka, and R. Wiesendanger, J. Magn. Magn. Mater. **240**, 64 (2002).

¹¹R. Wiesendanger and H. J. Güntherodt, Surf. Sci. **235**, 1 (1990).

¹²J. A. Stroscio, D. T. Pierce, A. Davies, R. J. Celotta, and M.

- Weinert, Phys. Rev. Lett. **75**, 2960 (1995).
- ¹³M. Bode, O. Pietzsch, A. Kubetzka, and R. Wiesendanger, J. Electron Spectrosc. Relat. Phenom. **114-116**, 1055 (2001).
- ¹⁴M. Bode, O. Pietzsch, A. Kubetzka, S. Heinze, and R. Wiesendanger, Phys. Rev. Lett. **86**, 2142 (2001).
- ¹⁵J. C. Slonczewski, Phys. Rev. B **39**, 6995 (1989).
- ¹⁶A. Hubert and R. Schäfer, *Magnetic Domains* (Springer, Berlin, 1998).
- ¹⁷H. P. Oepen and J. Kirschner, Phys. Rev. Lett. **62**, 819 (1989).
- ¹⁸M. R. Scheinfein, J. Unguris, R. J. Celotta, and D. T. Pierce, Phys. Rev. Lett. **63**, 668 (1989).
- ¹⁹J. P. Hill, G. Helgesen, and D. Gibbs, Phys. Rev. B **51**, 10 336 (1995).
- ²⁰K.-F. Braun, S. Fölsch, G. Meyer, and K.-H. Rieder, Phys. Rev. Lett. **85**, 3500 (2000).
- ²¹C. L. Fu and A. J. Freeman, Phys. Rev. B **33**, 1755 (1986).
- ²²We used the OOMMF program, release 1.2 alpha 2 (<http://math.nist.gov/oommf/>).
- ²³N. E. Christensen, O. Gunnarsson, O. Jepsen, and O. K. Andersen, J. Phys. (Paris), Colloq. **49**, C8-17 (1988).
- ²⁴D. van der Marel and G. A. Sawatzky, Phys. Rev. B **37**, 10 674 (1988).
- ²⁵G. Stollhoff, A. M. Oleś, and V. Heine, Phys. Rev. B **41**, 7028 (1990).
- ²⁶O. K. Andersen, O. Jepsen, and D. Götzel, *Highlights of Condensed Matter Theory*, edited by F. Bassani, F. Fumi, and M. P. Tosi (North-Holland, Amsterdam, 1985).
- ²⁷T. Shinjo, T. Okuno, R. Hassdorf, K. Shigeto, and T. Ono, Science (Washington, DC, U.S.) **289**, 930 (2000).
- ²⁸J. Raabe, R. Pulwey, R. Sattler, T. Schweinböck, J. Zweck, and D. Weiss, J. Appl. Phys. **88**, 4437 (2000).
- ²⁹A. Wachowiak, J. Wiebe, M. Bode, O. Pietzsch, M. Morgenstern, and R. Wiesendanger, Science (Washington, DC, U.S.) **298**, 577 (2002).
- ³⁰P. Evens, E. Isaacs, G. Aeppli, Z. Cai, and B. Lai, Science (Washington, DC, U.S.) **295**, 1042 (2002).